3D RANDOM WALK BASED SEGMENTATION FOR LUNG TUMOR DELINEATION IN PET IMAGING

D.P. Onoma [1,3] *S. Ruan*[1] *I. Gardin*[1,2] *G.A. Monnehan*[3] *R. Modzelewski*[1,2] *P. Vera*[1,2]

[1] LITIS EA 4108 - QuantIF, University of Rouen
[2] Department of nuclear medicine, centre Henri-Becquerel & LITIS EA 4108 - QuantIF
[3] LPNR, UFR-SSMT, University of Cocody, 22 BP 582 Abidjan 22, Côte d'Ivoire

ABSTRACT

This article presents a segmentation approach based on random walk (RW) method to delineate tumors having inhomogeneous activity distributions of ^{18}FDG on Positron Emission Tomography (PET) images. Based on the original algorithm of RW [1], we propose an improved approach using an adaptive parameter instead of a fixed one and integrating probability densities of label into the system of linear equations used in the RW. The proposed segmentation method initializes automatically seeds in tumor voxels using Fuzzy-C Means (FCM), and then delineates the tumor volume using the improved RW. The performances of the algorithm were assessed on PET images of a physical phantom, covering a range of hot spheres simulating tumor lesions of volume [0.99 - 97.3 mL] and contrast [2 - 7.7] for a voxel size of $4.1\times4.1\times2.0$ mm^3. A comparison study with a fixed threshold value of 40 % [2] and an adaptative thresholding algorithm [3] have been carried out. Results show that the proposed method is more effective than the other methodologies for spherical volume measurement. The good performances of the improved RW method have been also confirmed on data of three patients having heterogeneous ^{18}FDG uptakes.

Index Terms— Segmentation, random walk, 3D images, FCM, PET, tumor, uptake heterogeneity.

1. INTRODUCTION

For the definition of the target volume in radiotherapy, ^{18}FDG Positron Emission Tomography provides an additional metabolic information to anatomical images using computed tomography (CT). It provides a good detection and discrimination of tumoral tissues [4]. Numerous semi-automatic methods have been proposed to delineate FDG positive tissue, but it is still a problem to obtain an accurate tumor definition because of low quality of PET images due to low spatial resolution, noise, partial volume effect, some complex shapes of lesions and nonhomogenous uptake of FDG. Most current methods are based on thresholding, such as the used of a fixed threshold (40% to 50 % of the maximum value in the lesion) [2] and adaptive thresholding algorithms [3]. These methods, using only intensity, do not integrate spatial context of voxels. Adaptive thresholding methods require a calibration step on phantom, depending on acquisition parameters. A recent interesting adaptive local approach (3-FLAB) using a fuzzy concept was proposed to deal with heterogeneous uptake [5]. However it takes only intensity information. In the presence of necrotic area within the tumor, this method could not delineate correctly the whole tumor area.

We propose a PET segmentation method based on the random walk (RW) using a small set of pre-labeled voxels (seeds). Then, the other voxels are assigned to the label of the seed point that a random walker, starting from that voxel, would be most likely to be reached first. Thanks to the mathematical formulation of the probability of a walker in a neighborhood very close and the positions of the seed, the walker can go to object boundaries under some conditions. It provides a tool dealing with heterogeneous uptake on PET images. However, this method has some limitations, such as dependence to the choice of the free parameter, β, as well as the probability that a random walker going to a label, depending only on the gradient of intensity. Several papers [6, 7, 8] tried to improve its robustness but they do not deal with the dependance of β. To solve these problems, we propose an improved approach to make the parameter β adaptive and to integrate the probability of each label in the system of linear equations used in the RW.

The paper is organized as follow: Section 2 introduces review of the RW method. Section 3 presents our PET tumor segmentation method. Validation on phantom and patient's data is detailed in section 4. The discussion and conclusion are reported in section 5.

2. REVIEW OF THE RW METHOD

This algorithm, proposed by Grady *et al* [1], requires a small number of labeled voxels as an initial step. The segmentation is obtained by assigning each voxel a label, corresponding to

the greatest probability of a random walker, starting from this voxel to reach the label. In this approach, image is considered as a purely discrete object. So a graph, with a fixed number of nodes and edges, are created. The graph consists of a pair $G = (V, E)$ with nodes $v \in V$ and edges $e \in E$. An edge, e, spanning two nodes, v_i and v_j, is denoted by e_{ij}. The weight necessary for the walker's moving on this graph according to a connectivity follows the empirical function ω_{ij}, such as:

$$\omega_{ij} = exp[-\beta(g_i - g_j)^2] \tag{1}$$

where both g_i and g_j are the image intensity values at voxels i and j. β represents the free parameter depending on the user.

The probability that a random walker starting at a given unlabeled voxel will first reach a voxel of a particular label is computed, based on solving the so-called Dirichlet problem [1] with the boundary conditions given by seeds location.

A Dirichlet integral may be defined as:

$$D[\mathcal{U}] = \frac{1}{2}\int_{\Omega} |\nabla \mathcal{U}|^2 \, \mathrm{d}\Omega \tag{2}$$

for a field $\mathcal{U}$ and a region Ω. The solution is given by a harmonic function that satisfies the Laplace equation :

$$\nabla^2 \mathcal{U} = 0 \tag{3}$$

The Laplacian matrix can be defined as:

$$L_{ij} = \begin{cases} p_i & \text{if } i = j, \\ -\omega_{ij} & \text{if } v_i \text{ and } v_j \text{ are adjacent nodes,} \\ 0 & \text{otherwise} \end{cases} \tag{4}$$

with $p_i = \sum \omega_{ij}$ for each node v.

The Laplacian matrix is a sparse matrix. It can be built according to 4 or 8 connectivity for 2D images, and 6 or 26 connectivity for 3D images. It is partitioned into four sub matrices :

$$\begin{bmatrix} L_M & B \\ B^T & L_U \end{bmatrix} \tag{5}$$

in which, the subscripts M and U stand for marked, (labeled), and unmarked, (unlabeled), voxels. The Laplacian matrix defines a system of linear equations, which may be used to solve the following system (solving the Dirichlet problem) :

$$L_U \chi = -B^T M \tag{6}$$

L_U: Edge weights for the unlabeled voxels ($n_U \cdot n_U$);

M: Binary matrix of values 0 or 1 of size $n_M \cdot l$ (where l is the number of labels and n_M the number of seeds), corresponding to the boundary conditions of seeds;

B^T: Edge weights corresponding to the unlabeled and labeled voxels ($n_U \cdot n_M$);

χ: the probability for each voxel being a member of the labels ($n_U \cdot l$).

Using the probability, obtained by solving the system of linear equations 6, each voxel in the image is then assigned to its corresponding label for which it has the highest probability.

3. TUMOR SEGMENTATION METHOD

Our 3D tumor segmentation method is carried out in a region of interest (ROI). It can be separated in two steps. The first one corresponds to the definition of seeds (tumor and non tumor). The second one performs the proposed RW to delineate tumor in 3D.

3.1. Initialization of RW

To fastly solve the system of linear equations, a ROI including the tumor is defined on CT images of the patient. To initialize the method of RW, we firstly define seeds automatically. All the voxels of the outline of the ROI are considered as seeds of healthy tissues (background). The tumor seeds are defined automatically by the fuzzy C-means method [9]. Because of the heterogeneity of the grayscale in tumor, the voxels of the image are classified in 3 classes: background (C_1), moderate FDG uptake (C_2) and high uptake (C_3). The voxels of grayscale upper to middle of the centroid of C_2 and C_3 are defined as tumor seeds.

3.2. The improved RW method

To build the Laplacian matrix, we use 26 connectivity for the adjacency graph as shown in Figure 1. In 3D connectivity, there are 5 differents distances between adjacents nodes $(d_1 < d_2 < d_3 < d_4 < d_5)$.

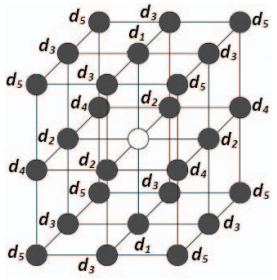


Fig. 1. Lattice neighborhood in 3D showing 5 differents distances when using 26 connectivity.

To overcome the character operator dependent of the free parameter β in equation 1, we propose to use the distance between adjacent nodes. Thus, the weight function in equation 1 becomes:

$$\omega_{ij} = exp[-(g_i - g_j)^2/(h_i - h_j)^2] \tag{7}$$

where the added $d = |h_i - h_j|$ represents the euclidean distance between adjacent voxels i and j. The weight function depending now not only on the intensity of grayscale, but also on the euclidean distance between adjacent voxels. It increases the weight of transition between two adjacent voxels similar in intensity but far in distance, maximizing the probability of the walker going to a seed.

After the automatic determination of seeds and modeling of their probability density as a Gaussian, each seed is associated to a function of probability density of label j, as follows:

$$\rho_j(I, \mu_j, \sigma_j) = 1/[\sqrt{2\pi} \cdot \sigma_j] \cdot exp[-(I - \mu_j)^2/2\sigma_j^2] \quad (8)$$

The submatrix B^T is then modified according to :

$$B'_{ij} = \rho_j \cdot B^T_{ij} \quad (9)$$

Thus, the connection between unlabelled voxels and seeds with high probability density ρ_j are strengthened. This allows to better classify unlabelled voxels. The system of linear equations becomes as follows :

$$L_U \chi = -B'M \quad (10)$$

4. VALIDATION

Our method has been carried out both on phantom and patients PET images. PET acquisition and image reconstruction were obtained on a Biograph Sensation 16 Hi-Rez PET scanner (Siemens Medical Solution, Knoxville, TN, USA) following the same clinical protocol. PET emission data were acquired in 3-dimensional mode with a 162 mm axial Field Of View (FOV). The acquisition was performed using emission scan of 3 min per bed position. Images were corrected for dead-time, random, scatter and attenuation, and reconstructed with AWOSEM (4 iterations and 8 subsets) in a 168×168 matrix (voxel size of 4.1×4.1×2.0 mm^3). A Gaussian post filtering was applied (FWHM = 5 mm). The spatial resolution was 4.4 mm in transverse plane at the center of FOV.

4.1. Phantom studies

The phantom was a cylindrical object (Data Spectrum Corporation, Hillsborough, NC, USA) containing 8 spheres of volume ranging from 0.99 to 97.3 mL. The ^{18}FDG has been included in the spheres and in the background of the cylinder according to radioactive concentrations used in clinical routine (Fig. 2). Data were acquired under 5 different contrasts between the spheres and background, ranging from 2 to 7.7 (2, 3.4, 4.9, 6.3 and 7.7).

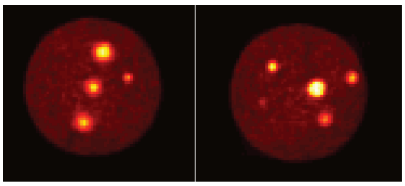
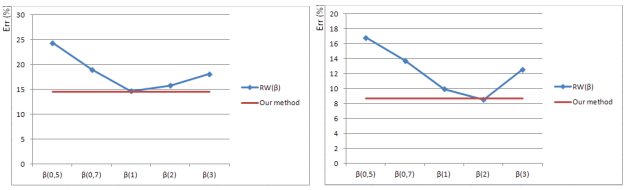


Fig. 2. Cylindrical phantom with different sizes.



(a) (b)

Fig. 3. Comparison of 2 differents methods from the average values of relative errors on small spheres (a) and large spheres (b) of cylindrical phantom.

4.1.1. *Comparison with the original RW method*

For evaluation, both the proposed and original methods were tested on the phantom. To avoid a methodological bias, the same initialisation step was used both for the RW(β) and our method. The original method of RW was performed using 5 β-values, ranging from 0.5 to 3. This range was chosen after a preliminary study on PET images. The relative errors on volume measurement (in %) were calculated. The results presented on figure 3 correspond to average errors on the small spheres ($Vr \leq 3.78$ mL) and large spheres ($Vr \geq 11.6$ mL) for both methods. This figure shows that the relative error increases when β-value is inferior to 1 and superior to 2. The original algorithm is close to our method when β=1 for small spheres and when β=2 for large spheres. It is very sensitive to the choice of β-value, whereas our method is stable and more efficient.

4.1.2. *Comparison with other methods*

A comparison was performed between our method, a recent adaptive thresholding method [3] (TAD) and the use of a fixed threshold value corresponding to 40 % (T40%) of the maximum value in the lesion. These two methods were chosen because the recent adaptive thresholding method presents better results than other methods in [3] and thresholding fixed to 40% is usually used in clinical routine. The results in table 1 show that our method gives better performances than others whatever the size of the sphere. It can be also observed that all methods make high errors in small spheres due to partial volume effect.

Method	Err(%) small spheres	Err(%) large spheres
T40%	58.0±18.5	27.3±2.8
TAD	31.7±18.2	12.8±2.6
Our method	30.9±3.8	10.8±6.4

Table 1. Comparison of 3 methods measurement of volume by the mean error and standard deviation for small spheres ($Vr \leq 3.78$ mL) and large spheres ($Vr \geq 11.6$ mL).

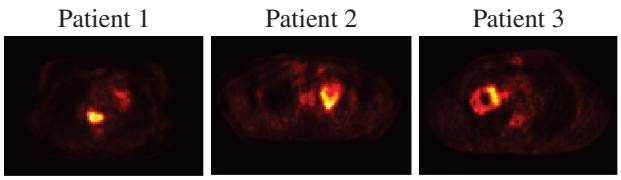


Fig. 4. PET images showing 3 patients with lung cancer.

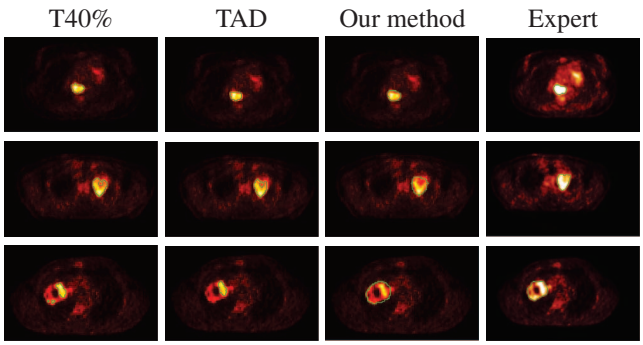


Fig. 5. Segmentation results (green contour) on patient 1, 2 and 3 on lines 2 to 4 respectively: columns 1 to 4 show the segmentation obtained by each method.

4.2. Patient studies

The performance of the 3 methods (our method, TAD and T40%) were also evaluated on PET images of 3 patients with lung cancer (Fig.4). The results are shown in Figure 5. The 3 tumoral volumes (TV) manually delineate by expert were 30.7 mL, 49.3 mL and 159.6 mL. Our method gives results (in %) close to the expert (2.5, 3.0 and 7.3), whereas T40% (-20.6, -49.1 and -63.5) and TAD (-23.4, -53.1 and -60.3) underestimate TV. Both methods (TAD and T40%) do not provide a satisfactory segmentation because of heterogeneous uptake in lesions mainly in area when the tumor is necrotic. When the heterogeneity is significant, these two methods lead to undervaluation of TV because they tend to extract only the high uptake region (e.g., Fig. 5, Patients 2 and 3). Our method is able to segment the whole lesion including necrosis.

5. DISCUSSION AND CONCLUSION

The choice of β influences the weight of walker. Indeed, a high β-value reduces the weight, which weakens the connection between the adjacent voxels and underestimates the TV. Conversely a low β-value increases the weight, which overestimates the volume. On phantom data our improvement gives better results than the original method while avoiding the choice of β.

For functional volume delineation, segmentation methods in clinical practice are usually based on a fixed or adaptive thresholding. These algorithms have shown an acceptable delineation under specific conditions such as cylindrical phantom case and when the activity distribution is homogeneous. In clinical practice the lesions have often complex shapes and nonhomogeneous uptake. In these cases, these methods fail by undervaluation of the lesion. Our method which takes into account these problems allowing to obtain a better delineation could be greatly beneficial for radiotherapy treatement. Our study was performed only on a small sample of patients and these results need to be confirmed in a larger group of patients.

6. REFERENCES

[1] L. Grady, "Random walks for image segmentation," *IEEE Trans Pattern Anal Mach Intell*, vol. 28, pp. 1768–1783, Nov 2006.

[2] Y. E. Erdi, O. Mawlawi, S. M. Larson, M. Imbriaco, H. Yeung, and R. Finn, "Segmentation of lung lesion volume by adaptive positron emission tomography image thresholding," *Cancer*, vol. 80, pp. 2505–2509, 1997.

[3] S. Vauclin, K. Doyeux, S. Hapdey, A. Edet-Sanson, P. Vera, and I. Gardin, "Development of a generic thresholding algorithm for the delineation of ^{18}FDG-PET-positive tissue: application to the comparison of three thresholding models," *Phys Med Biol*, vol. 54, pp. 6901–6916, Nov 2009.

[4] S. S. Gambhir, J. Czernin, J. Schwimmer, D. H Silverman, R. E Coleman, and M. E Phelps, "A tabulated summary of the FDG PET literature," *J Nucl Med*, vol. 42, pp. 1S–93S, 2001.

[5] M. Hatt, C. Cheze le Rest, P. Descourt, A. Dekker, D. De Ruysscher, M. Oellers, P. Lambin, O. Pradier, and D. Visvikis, "Accurate automatic delineation of heterogeneous functional volumes in positron emission tomography for oncology applications," *J Radiat oncol Biol Phys*, vol. 77, pp. 301–308, 2010.

[6] M.-P. Jolly and L. Grady, "3D general lesion segmentation in CT and validation," in *Biomedical Imaging 5th International Symposium*. IEEE, 2008, vol. 4, pp. 796–799.

[7] C. Chefd'hotel and A. Sebbane, "Random walk and front propagation on watershed adjacency graphs for multilabel image segmentation," in *11th International Conference on*. IEEE, 2007, vol. 7, pp. 1–7.

[8] R. Rzeszutek, T. El-Maraghi, and D. Androutsos, "Image segmentation using scale-space random walks," in *16th International Conference on Digital Signal Processing*. IEEE, 2009, vol. 4, pp. 1–4.

[9] J. C. Bezdek, *Pattern Recognition with Fuzzy Objective Function Algorithms*, Kluwer Academic Publishers, 1981.